Characterization of atherosclerosis plaques by measuring both backscattering and attenuation coefficients in optical coherence tomography

Chenyang Xu
Joseph M. Schmitt
Lightlab Imaging Inc.
1 Technology Park Drive
Westford, Massachusetts 01886
E-mail: xuchenyang@gmail.com

Stephane G. Carlier
Cardiovascular Research Foundation
55 East 59th Street
New York, New York 10022

Renu Virmani
CVPath Institute
19 Firstfield Road
Gaithersburg, Maryland 20878

Abstract. Intravascular optical coherence tomography (OCT) has been proven a powerful diagnostic tool for cardiovascular diseases. However, the optical mechanism for the qualitative observations are still absent. We address the fundamental issues that underlie the tissue characterization of OCT images obtained from coronary arteries. For this, we investigate both the attenuation and the backscattering properties of different plaque components of postmortem human cadaver coronary arteries. The artery samples are examined both from lumen surface using a catheter and from transversely cut surface using an OCT microscope, where OCT images could be matched to histology exactly. Light backscattering coefficient μ_b and attenuation coefficients μ_t are determined for three basic plaque types based on a single-scattering physical model: calcification ($\mu_b=4.9\pm1.5$ mm^{-1}, $\mu_t=5.7\pm1.4$ mm^{-1}), fibers ($\mu_b=18.4\pm6.4$ mm^{-1}, $\mu_t=6.4\pm1.2$ mm^{-1}), and lipid pool ($\mu_b=28.1\pm8.9$ mm^{-1}, $\mu_t=13.7\pm4.5$ mm^{-1}). Our results not only explain the origins of many qualitative OCT features, but also show that combination of backscattering and attenuation coefficient measurements can be used for contrast enhancing and better tissue characterization. [DOI: 10.1117/1.2927464]

Keywords: optical coherence tomography; attenuation; backscattering; atherosclerosis; plaque; tissue characterization.

Paper 07416R received Oct. 4, 2007; revised manuscript received Jan. 4, 2008; accepted for publication Jan. 31, 2008; published online Jun. 5, 2008.

1 Introduction

The rupture of thin-cap fibroatheroma (TCFA), the preponderant histological type of the suspected "vulnerable plaque," is believed to account for more than half of the acute myocardial infarctions in human.[1] Pathologically, the TCFA is currently defined as a lesion with a thin, macrophage-rich fibrous cap (<65 μm) overlying a large lipid-rich core.[2] Identification of TCFA and other rupture-prone lesions would advance our understanding of the atherosclerosis process and facilitate the development of therapeutic interventions. However, most *in vivo* imaging modalities, including intravascular ultrasound (IVUS), computer tomography (CT), and magnetic resonance imaging (MRI), are currently limited by a resolution less than 100 μm and are unable to detect TCFA reliably.

Intravascular optical coherence tomography (OCT) is a catheter-based, high-resolution imaging method that has demonstrated considerable application for both coronary artery and periphery artery imaging.[3–6] The state-of-art intravascular OCT system now in clinical use can deliver 10 to 20-μm resolution with 0.5 to 2-mm penetration depth. Recently, high-speed OCT systems have been developed that can acquire OCT images at line rates exceeding 370,000 lines/s, making it possible to image a complete artery volume in a few seconds.[7,8] Due to its high resolution, OCT is considered to be the most promising imaging modality for detecting the TCFA *in vivo* as well as for studying its natural progression.[9]

OCT tissue characterization was first carried out by imaging the artery samples from the lumen side using either a rotary probe or microscope and comparing the OCT images to the matched histology. In earlier studies, the main features of OCT images of different types of atherosclerotic plaques were identified by histological correlation. Each of the three major plaque types is characterized by a specific set of features: fibrous plaques appear as a homogeneous signal-rich regions, lipid plaques as signal poor regions with diffuse borders, and calcified plaques as sharply delineated signal-poor regions with islands of signal-rich regions.[4,5] These features had been successfully utilized for many *in vivo* diagnostics.[5,6,10,11] However, the fundamental physical explanations for the observations have not been formulated. Without such explanations, OCT images are prone to misinterpretation. For example, in intensity-only OCT images, to account for the low-signal appearance of lipid plaques, it has been believed[3,4,12,13] that the lipid tissue exhibits low optical reflectance, while fibrous tissue exhibits high optical reflectance in OCT. However, if this is the case, the diffuse lipid margins in OCT imply

Address all correspondence to Chenyang Xu, Lightlab Imaging Inc., 1 Technology Park Drive, Westford, MA 01886; Tel: (978)399–1091; Fax: (978)692–3689; E-mail: xuchenyang@gmail.com

1083-3668/2008/13(3)/034003/8/$25.00 © 2008 SPIE

gradual transition from fibrous tissue to lipid tissue, which contradicts the fact that most margins of lipid plaque are sharply delineated in histology.[14]

With the goal of enhancing tissue discrimination, there has been a growing interest in exploiting the quantitative measurement of the optical properties of atherosclerotic plaques. It was shown[15] with tissue phantoms that OCT is capable of measuring scattering coefficients with high precision ($>0.8\%$). Levitz et al. first performed quantitative analysis of scattering coefficients and anisotropy factors from human artery samples.[13] Their study indicated that differences exist in optical properties between normal and atherosclerotic plaques. Later, van der Meer et al. demonstrated that such analysis can be done with spatial localization, and therefore, is applicable to different tissue layers.[16,17] However, in most previous studies, tissue discrimination was performed using only one optical parameter. There were significant overlaps of the measured parameter ranges for different tissue types measured by different groups. This renders tissue classification based on quantitative measurement inaccurate. In addition, there are discrepancies in the reported measurement results due to factors such as different light sources and different physical models used.

Ideally, to ensure good separation, individual plaque components should be isolated and their optical properties should be measured. However, because of their convoluted geometry and weak mechanical integrity, individual plaque components, such as lipid and fibrous tissues, are difficult to isolate without major tearing or deformation. Therefore, in previous OCT studies, imaging of coronary arteries was performed on intact arteries from the lumen side. Luminal imaging poses a serious limitation for basic studies of optical properties of coronary plaques because histological sections cannot be matched exactly to corresponding OCT images, and often, because of limited optical penetration, the full radial extent of lipid plaques cannot be imaged. In luminal imaging, the tissue properties extracted from deeper tissue layers may be influenced by overlying tissue layers and hence may be inaccurate. These limitations could have also contributed to the different measurement results in the past studies.

With the goal of facilitating *in vivo* OCT tissue characterization, we investigated both the basic backscattering and attenuation properties of fibrous, lipid, and calcified plaques. To overcome the limitations of previous studies, in addition to conventional OCT imaging from the luminal side of the artery, we performed OCT microscope scans in the transverse plane by sectioning the artery and viewing it on end, where exact matching of histology to OCT is much easier and the heterogeneous regions of the plaque can be segmented visually. The microscopic variations of the optical properties of different plaques types were measured. Based on these measurements, the concept of plaque characterization by combining backscattering and attenuation measurements is introduced. The results explain the basic physics of OCT that generate contrast among fibrous, lipid, and calcified plaques. Finally, the significance of our findings with respect to vulnerable plaque identification is discussed.

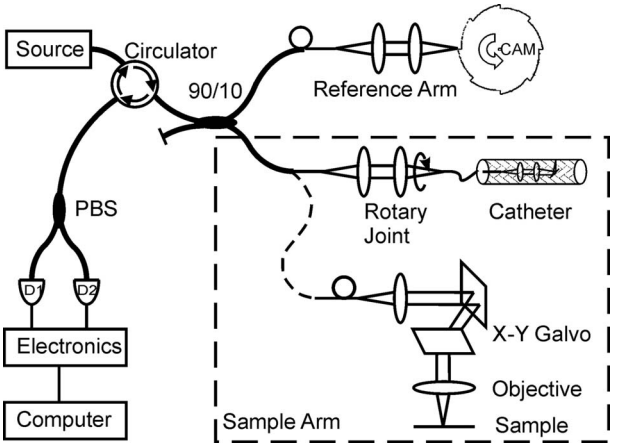

Fig. 1 Schematic of the time-domain mixed OCT system used in the experiment. Broadband light from broadband sources (λ_c=1310 nm, $\Delta\lambda$=105 nm) passes through a 90/10 optical splitter into the reference and sample arms. The key component of the reference arm is a rotating multifaceted cam-shaped reflector. The sample arm is either an imaging catheter with a rotating probe (rotary scanning) or a microscope with *x-y* beam scanning mechanisms (transverse scanning). To implement the polarization diversity, the two orthogonal polarization states are separated by a polarizing beamsplitter (PBS) and detected by photodiodes D1 and D2 separately. The signals are processed and digitized by electronic circuits and computer for real-time display and data storage.

2 Methods

2.1 *OCT Systems*

The OCT system used for transverse scanning of cross-cut arteries (Fig. 1) is a custom-built dual-source broadband 3-D OCT scanning microscope (Lightlab Imaging Inc., Westford, Massachusetts) with a center wavelength of 1320 nm. The sample arm consists of a large-diameter, low-numerical-aperture microscope objective and an *x-y* scanning assembly with scanning range up to 2×2 cm. It provides an axial resolution of 7.3 μm in air (5.4 μm in tissue) and a lateral resolution around 25 μm. In these studies, the sampling density was set to 2.1 μm for the axial direction and 12 μm for both lateral directions. The OCT system used for conventional rotary scanning from lumen is a standard cardiovascular OCT system modified for operation with broadband superluminescent laser diodes (CV-M2 System, Lightlab Inc., Westford, Massachusetts). The specially-built OCT catheter for *in vitro* rotary imaging consisted of a rotating optical fiber with a microlens at its tip, placed inside a water-flushed sheath with an outer diameter of 0.9 mm. Because the fiber optic rotary joint introduces an additional transmission loss, and the collection efficiency of the rotary probe is somewhat less than the microscopic lens, samples of same backscattering intensity may produce different measurements for the scanning microscope system and the rotary system. This efficiency difference was calibrated by imaging 0.03% 0.2-μm polystyrene microsphere solution (Polysciences Inc., Warrington, Pennsylvania).

2.2 *Specimens and OCT Imaging*

Human coronary arterial segments (N=72) were obtained from anonymous autopsy examinations, less than 12 h past

death at the New York Presbyterian Hospital/Columbia University Medical School ($N=29$). To prevent artery contraction and deformation, the hearts were pressure-fixed before excision using 10% formalin, recirculating at 100 mmHg for 2 h. Artery segments presenting significant plaque accumulation were identified and excised. During OCT imaging, the artery segments were immersed in a bath of 0.9% NaCl solution maintained at 37°C. The arteries were first imaged with a rotary catheter to identify the regions of interest and to identify possible loci of large lipid or fibrotic plaques. Nineteen artery segments were cut transversely at selected locations normal to the artery axis to expose 33 cross sections. The arteries were then imaged with the 3-D OCT scanning microscope. The cut surface was oriented normal to the imaging beam. With a thin layer of saline left covering the cut surface to act as index-matching fluid, the focus of the microscope objective was adjusted to the top surface of the tissue. The position of the laser beam on the tissue was monitored by a visible aiming beam (Fig. 1). After imaging all artery samples, a tissue phantom composed of 0.03% 0.2-μm polystyrene microsphere solution was imaged using the same settings as the arteries to calibrate intensity variations with depth caused by lens defocusing and other artifacts for both the rotary imaging system and the transverse imaging system.

The wall of the normal artery is a layered structure with a distinctive pattern of cells and extracellular matrix (e.g., collagen and elastin). This highly ordered structure is anisotropic and its optical properties may depend on the direction of OCT probing beam. Therefore, a series of experiments were performed in large plaques to analyze whether the optical properties of different artery wall and plaque components depend on the angle of incidence of the probe beam. The arteries were mounted to tilting stage and backscattering and attenuation data were collected from large plaque volumes (0.25×0.25-mm^2 square) for different tilt angles of the artery. For the tilt angle of 90 deg, the arteries were imaged from the lumen side with a catheter.

2.3 *Histology*

After OCT imaging, the samples were embedded in paraffin with the cut surface parallel to the cutting blade. The uppermost complete tissue slices were used for histology staining with hematoxylin & eosin (H&E), Movat, and picrosirius red. Using artery landmarks near the cut surface, the transverse OCT image, the rotary OCT image, and the histology were matched. The rough tissue characterization was identified in the OCT images using published qualitative findings.[4,12]

2.4 *Signal Processing*

The OCT data were first corrected for any aberration and focusing effect using the intensity profile obtained from the phantom image. Based on the histology, regions of interest (ROIs) are identified such that each ROI only included one type of tissue. Quantitative analysis of tissue backscattering and attenuation of the OCT images were performed for the identified ROI on OCT microscopy data. Average axial scans were obtained from an *en face* 0.25×0.25-mm^2 square (400 axial lines) in the ROI. OCT signals were assumed to be spatial distributions of signal corrupted by additive random noise. The noise floor was identified and subtracted from OCT signal. For model fitting, 50 μm (about nine coherence lengths in tissue) below the specular reflection peak was chosen as the starting depth, and the point where the signal attenuated to 37% $(1/e)$ of the starting point was chosen as the ending depth. In this region, the power signal $P(z)$ from tissue mostly follows the first-order scattering approximation, and can be modeled as an exponentially decaying function:[18]

$$P(z) \approx \tfrac{1}{2} P_i \mu_b L_c A(z) \exp(-2\mu_t z/n), \tag{1}$$

where P_i is the incident laser power, μ_b is the backscattering coefficient, L_c is the coherence length of laser source, $A(z)$ is the beam-divergence function, μ_t is the total attenuation coefficient, and n is the refractive index of the tissue. For artery tissue, the attenuation coefficient μ_t is dominated by scattering loss. For this study, the refractive indices of fibrous tissue, lipid pool and calcification were assumed to be 1.35, 1.43 and 1.50, respectively.[19] Since the dilute microsphere phantom had very low attenuation coefficient (i.e., $\mu_t(z) \ll 1$ mm^{-1}), the power signal $P_0(z)$ backscattered from the microsphere phantom can be modeled as

$$P_0(z) \approx \tfrac{1}{2} P_i \mu_{b0} L_c A(z), \tag{2}$$

where μ_{b0} is the backscattering coefficient of the microsphere phantom. We calibrated μ_{b0} by comparing the OCT signal strength to that of a known reflector (e.g., reflection from a mirror attenuated by a calibrated neutral density filter). Taking the ratio of Eq. (1) to Eq. (2), and taking the logarithm of both sides, we have

$$\log(P(z)/P_0(z)) = \log(\mu_b/\mu_{b0}) - 2\mu_t z/n. \tag{3}$$

The backscattering coefficient μ_b and attenuation coefficient μ_t were obtained by least-squares line fitting using Eq. (3). The correlation coefficient R^2 was calculated and the fitting was inspected visually to verify the quality of the fit ($R^2 > 0.97$).

3 Results

3.1 *Applicability of the Transverse OCT Scanning Model*

The optical properties of all pathological plaque types, including fibrous caps and lipid plaques, showed little dependence on incident angles (Fig. 2). In contrast, the media showed large backscattering and attenuation variations when imaging from lumen side compared to imaging from the transverse direction. The optical angular anisotropy of the media is likely to result from the highly organized fibrous structure in the muscle layer.[20] This may account for media's different apparent intensity during *in vivo* imaging when the imaging catheter is passing through a curved artery segment. Since media is not the emphasis of this study, we conclude that the backscattering and attenuation measurements from fibrous caps and lipid plaques in the cross-cut arteries should represent those encountered *in vivo*, in spite of the different directions of incidence of the probing beams.

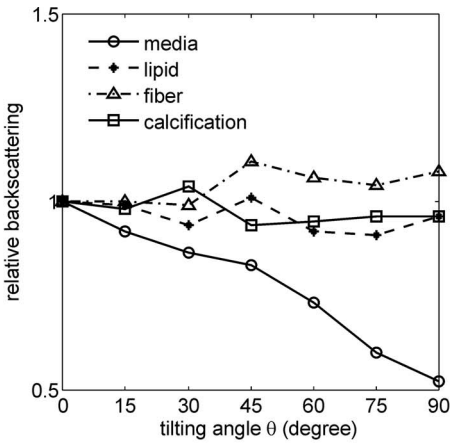

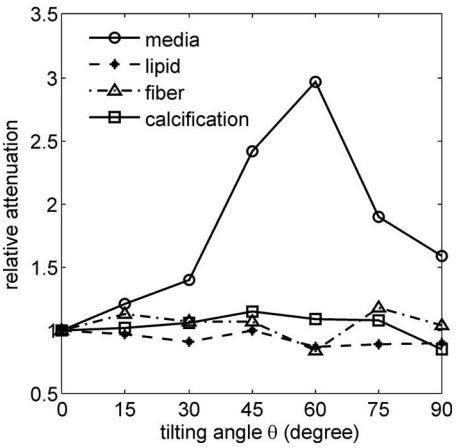

Fig. 2 Angular dependence of OCT backscattering and attenuation coefficients for different atherosclerosis plaque components.

3.2 *Transverse OCT Imaging Examples*

Figure 3 shows reconstructed rotary OCT scanning images, transverse OCT scanning images at 50 and 500 μm below surface, and corresponding histology of a representative fibroatheroma and a fibrocalcific plaque. With both OCT systems, different features of the atherosclerotic plaques could be identified. In rotary OCT scanning, the appearance of different tissue types matches previous descriptions.[4] The border between fibrous tissue and lipid tissue appears diffuse, making it very difficult to delineate the lipid plaque boundaries precisely based on intensity alone. In contrast, the same border appears sharp in both side-scanning OCT and histology. The lipid plaque is signal-rich in the upper layers, indicating a high backscattering coefficient. In fact, lipid region appears even brighter than most fiber regions in the upper layers. It becomes signal-poor only in deeper layers as a result of higher signal attenuation. The calcific plaque, on the other hand, appears signal-poor throughout the OCT penetration depth except the specular reflection at the very top. Furthermore, the media appears as signal-rich annulus in transverse scanning, while signal-poor in the rotary scanning. This is consistent with the result from the angular dependency studies.

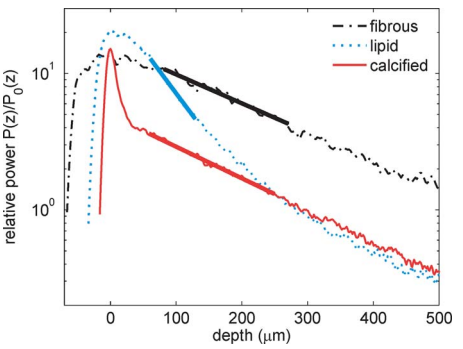

Fig. 4 Representative backscattered power curves for calcific, fibrous, and lipid tissues. The thick solid lines denote the model-fitting regions for optical parameters calculation.

3.3 *Optical Properties Measurement and Visualization in Transverse Scanning*

Figure 4 shows examples of averaged backscattered power curves from representative lipid, calcium, and fibrous plaques. Note that the curves were corrected for beam profile and aberrations by normalizing to the intensity obtained from the microsphere phantom. The peak at the zero depth in each of the curves was caused by specular reflections at the interface between the artery and surrounding liquid (saline). The remaining parts the curves appear smooth, indicating the imaged regions were relatively homogeneous. In weak-signal regions, some curvature is evident, suggesting an increasing effect of multiple scattering in deeper structures. We can see that compared to fibrous plaque, the lipid plaque exhibits both higher backscattering and higher attenuation. The lipid had higher signal strength than fibrous plaque at the top surface; however, the signal attenuates very fast and drops below fiber plaque around 50 to 100 μm. This also shows the effects of multiple scattering regions much earlier than the fiber. The calcified plaque showed both low backscattering and low attenuation, except in the shallow specular reflection region. The mean attenuation and backscattering coefficients for different plaque components are summarized in Table 1. The lipid tissue has higher backscattering and high attenuation coefficient than fibrous tissue ($p<0.0001$ and $p<0.0001$, respectively).

Since we had a 3-D image set, we can calculate the attenuation and reflectivity for every *en face* point and generate backscattering and attenuation maps (Fig. 5). These maps and the results in Table 1 indicate that better tissue characterization can be obtained by combining reflectivity and attenuation measurements. In the backscattering map, the fibrous tissue

Table 1 Optical backscattering and attenuation coefficients of three plaque types.

Plaque Type	N	μ_b (mm^{-1})	μ_t (mm^{-1})
Fibrous	23	18.6±6.4	6.4±1.2
Lipid	19	28.1±8.9	13.7±4.5
Calcified	14	4.9±1.5	5.7±1.4

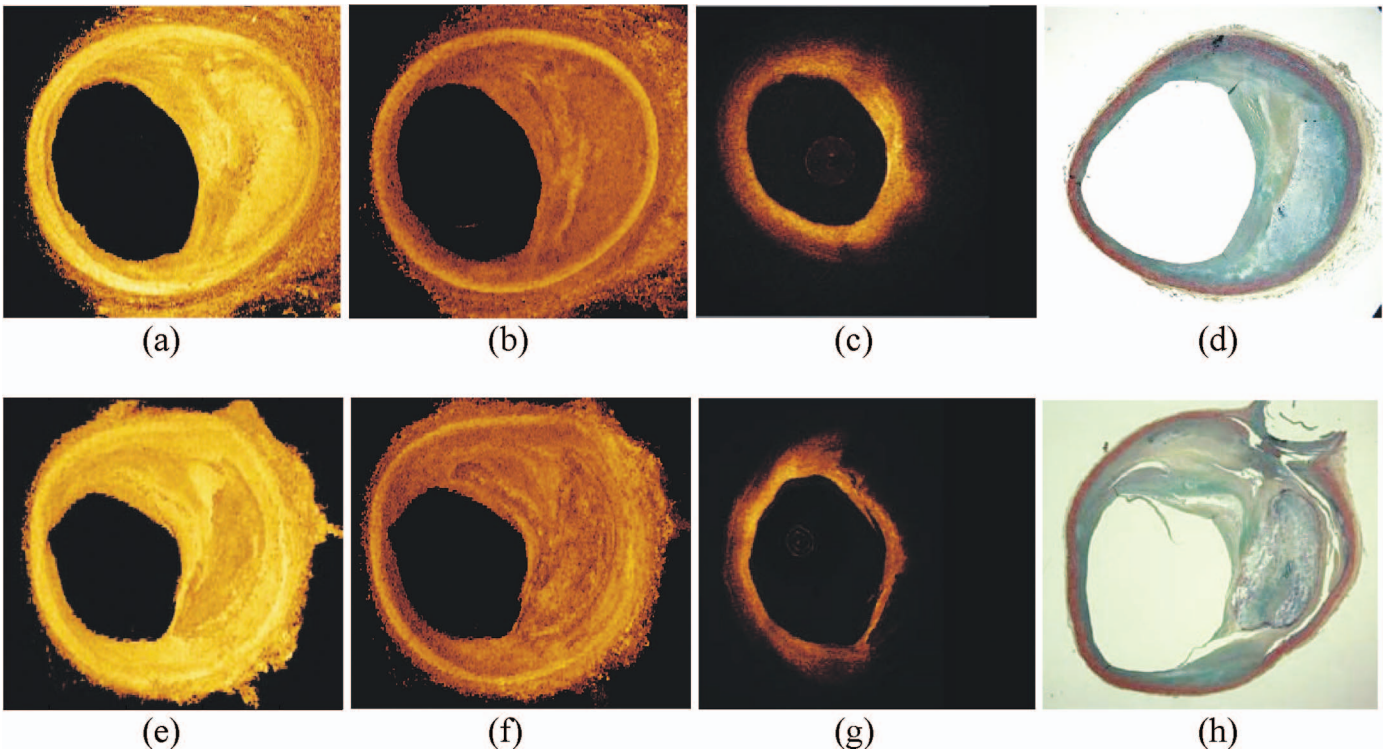

Fig. 3 Transverse OCT image at (a) and (e) 50 and (b) and (f) 500 μm below surface, (c) and (g) corresponding rotary OCT image and (d) and (h) corresponding histology (Movat's pentachrome) for a representative fibrolipid plaque (top row) and a fibrocalcific plaque (bottom row). A consistent color mapping was used for (a), (b), (c), (e), (f), and (g).

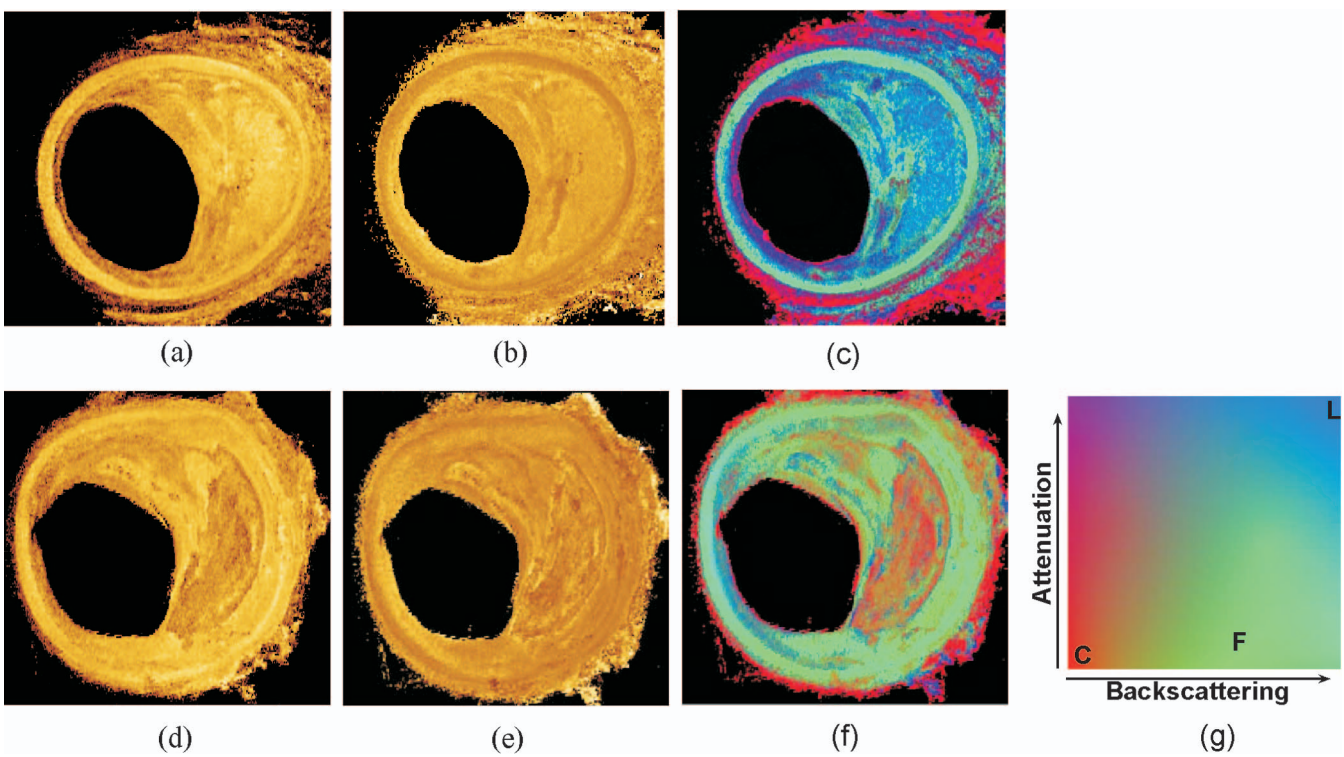

Fig. 5 (a) and (d) Backscattering and (b) and (e) attenuation images corresponding to the artery segments in Fig. 3 (top row: fibrolipid; bottom row: fibrocalcification). (c) and (f) Images combining backscattering and attenuation measurement using colormap defined in (g) and (g) colormap for combining the backscattering and attenuation measurements. Letters C, F, and L denote the positions of the average backscattering and attenuation coefficients for calcific, fibrous, and lipid tissue, respectively.

and the lipid tissue both show strong intensity, while the calcification shows weak intensity. In the attenuation map, the fibrous tissue and the calcification both showed weak intensity, while the lipid tissue shows strong signal. It is difficult to distinguish the three plaque types based on either property alone. However, it is possible to distinguish them based on both. Figure 5(g) shows a possible color mapping based on the combination of attenuation and backscattering. The calcification, which shows low backscattering and low attenuation regions, is mapped as red. The fibrous plaque, which has high backscattering and low attenuation, is mapped as green. The lipid plaque, which has high backscattering and high attenuation, is mapped as blue. Some intima regions having low backscattering and high attenuation were mapped as purple. Figures 5(c) and 5(f) show great contrast enhancement can be obtained using this approach to visualize the three plaque types.

4 Discussion

In the study reported here, the backscattering coefficients and attenuation coefficients of atherosclerosis plaques were measured by transverse imaging of transversely cut arteries using a high-resolution OCT microscopic system. Our experiments demonstrated that combining backscattering and attenuation measurements offers better plaque discrimination and improves plaque visualization.

4.1 *Interpretation of Plaque Components in OCT*

Our results address the optical properties that underlie the appearance of images acquired from intravascular OCT. The homogeneous and signal-rich appearance of fibrous tissue is due to their low attenuation and high backscattering coefficients. Qualitative studies showed that both calcified deposits and lipid pools appear as signal-poor regions in the OCT images, and the best visual cue that has been identified thus far for distinguishing them is border sharpness. The borders of calcified plaques are well-delineated and those of lipid pools are diffuse. Our results not only confirm the effectiveness of this visual cue, but also explain the origin of this border phenomenon. Because the calcium deposit has a low backscattering coefficient compared to that of fibrous tissue the OCT signal drops suddenly at the borders. In theory, the signal drops with in one coherence length (about 5 to 10 μm). In addition, because of the high refractive-index mismatch between the fiber and the calcification, the interface produces a specular reflection, which further increases the border contrast. On the other hand, because there is little difference between backscattering coefficients for fibrous and lipid tissue, the anatomical border between fibrous tissue and lipid pool cannot be distinguished based on intensity image alone. In fact, most lipids, especially those having foam cells on the top, have higher backscattering coefficients. Because the lipid has much higher attenuation coefficients than fibers, the signal attenuates very fast, and soon drops below the noise floor of the OCT system. At this point, the image contrast is lost and the deeper part of lipid plaque is indeed "signal-poor."

By looking at the electromicrograph images, we found that the lipid plaques and the foam cells are predominantly composed of relatively large particles close to probing light wavelength (0.5 to 5 μm), while the fibrous plaques are composed of fiber bundles of smaller size. The refractive index difference between lipid and the surrounding media is also larger than the hydrated fibers to the surrounding media.[19] These particles in lipid plaque behave like "Mie scatterers," where the light is mostly forward scattered. We speculate this high refractive index difference, combined with predominant forward scattering, is giving the lipid plaque the characteristic high backscattering and a high attenuation in OCT.

4.2 *Fiber-Lipid Boundary Detection and Implication to Vulnerable Plaque Identification*

An important application of intravascular OCT is for the detection of TCFA, the most important type of vulnerable plaques.[1] Currently, a TCFA is defined as a thin fibrous cap ($<$65 μm) overlying a large lipid pool.[2] OCT is considered the only method that can directly measure the fibrous cap thickness.[10,21] From our analysis, the apparent "border" between fiber and lipid (where the signal dropping below noise floor in OCT intensity image) is not the real anatomical border. The real location of anatomical border is inside the signal-rich region and can only be resolved by other means. It has been proposed using polarization-sensitive detection as means to distinguish collagen fiber from other tissue.[22,23] However, optical birefringence is difficult to measure during intravascular imaging because of rapid polarization fluctuations induced by rotation and stretching of fiber optic probes. In addition, the birefringence effect may be not strong enough to induce sufficient contrast within very thin fibrous tissue layers. In this paper, we introduce an alternative method, combined attenuation/backscattering measurement, which can be implemented in standard OCT systems that do not have polarization measurement capabilities.

4.3 *Plaque Isolation and Heterogeneity*

It is essential to be able to exactly match the histology to OCT images for OCT tissue characterization. In the past, most studies on coronary arteries were performed by scanning the tissue from the lumen side. However, because of the high aspect ratio of plaques (length along artery axis versus thickness along artery radius), it is very difficult to match tissue by simple geometrical measure if no clear landmark is present. *En face* scanning of cross-cut arteries provides distinctive advantages in the study of the basic optical properties of coronary plaques. First, it eliminates the problems of interpretation that arise from the shadowing effect of highly attenuating structures in plaques. Second, the removal of overlying tissue makes the identification of boundaries between plaques trivial, thereby making the OCT-histology matching much more accurate. Third, because of the elongated shape of most plaques, it is possible to obtain tissue optical properties by averaging over large homogeneous volumes, improving the measurement precision. Due to these advantages, we believe our studies yield a more definite measurement of optical properties of atherosclerotic components.

Despite the great improvement and extensive averaging, we still observe substantial standard deviations in the tissue optical properties measurements as well as coherent noise (speckle) effects. We believe this is mainly due to the com-

plexity of atherosclerotic plaques, both in chemical composition and microscopic physical organization. Moreover, there are mixed plaque types such as fibrofatty plaque and fibrocalcific plaque. The exact ratio of each component is expected to influence its optical properties. In addition, macrophage foam cells, which can be either dispersed or clustered, change the optical properties of tissue dramatically. In general, the foam cells were found to increase both the backscattering and attenuation coefficients. In this study, we chose three most basic plaque types. It is expected that finer classification categories incorporating composition differences and macrophage content will reduce the standard deviation of optical properties measurements.

4.4 *Study Limitations*

One limitation of the study reported here is the use of formalin-fixed cadaver specimens, which was required for cross-cutting a flat surface and accurate histology matching. Minor tissue changes may have occurred postmortem. While it is impossible to perform OCT imaging comparison before and after death, little changes were found in OCT images before and after formalin fixation (data not shown). In addition, numerous OCT cases performed in patients have shown that the OCT images of coronary arteries in vivo demonstrate features similar to those identified *in vitro*.[4,21] Therefore, it is likely that the quantitative measurement taken *in vitro* are applicable to those obtained *in vivo*.

Time-domain OCT system was used in this study because time domain system offers better image quality in the expense of slower imaging speed.[24] Because there is no fundamental difference between time-domain OCT and frequency domain OCT, we expect our conclusions will still hold if the data are acquired using a frequency-domain system. A single scattering model was used here due to its robustness and simplicity. In the transverse scanning OCT study, the fitting was obtained from the lumen surface to the $1/e$ attenuation depth, which corresponds to the mean free path (MFP) for single-scattered photons. It has been established that within one MFP the single-scattering model is valid, which is evident from our near-perfect model fittings. However, during rotary OCT imaging, plaques are on top of each other, and it might not always be possible to select regions that fits single-scattering model. In this situation, more sophisticated models incorporating multiple scattering effects will be more appropriate. In addition, attenuation measurement involves model fitting over certain tissue area. Even with the high-resolution system ($\sim 5\ \mu$m in tissue) employed in this study, a minimum tissue thickness of at least $40\ \mu$m was required for sufficient speckle reduction to improve measurement reliability. This reduced the spatial resolution of the optical parameter extraction. Many artifacts such as catheter uniformity, polarization effect, and blood clearance are also known to influence the reproducibility of the measurement of optical coefficients with OCT.

5 Conclusions

Combining measurements of optical backscattering and attenuation coefficients enhances differentiations between fibrous, lipid, and calcific plaques. Our results explained the optical basis behind many previously reported qualitative findings and revised the results of pioneering quantitative studies. This will contribute to future computer-aided diagnosis of atherosclerotic plaques and better detection of TCFA.

Acknowledgments

The work was supported by a research grant from Goodman Inc. The authors wish to thank Allen Burke, MD, for advices on histological processing and interpretation, and Amin Katouzian for helping in tissue sample collection.

References

1. E. Falk, P. K. Shah, and V. Fuster, "Coronary plaque disruption," *Circulation* **92**(3), 657–671 (1995).
2. R. Virmani, F. D. Kolodgie, A. P. Burke, A. Farb, and S. M. Schwartz, "Lessons from sudden coronary death: a comprehensive morphological classification scheme for atherosclerotic lesions," *Arterioscler., Thromb., Vasc. Biol.* **20**(5), 1262–1275 (2000).
3. M. E. Brezinski, G. J. Tearney, B. E. Bouma, J. A. Izatt, M. R. Hee, E. A. Swanson, J. F. Southern, and J. G. Fujimoto, "Optical coherence tomography for optical biopsy. Properties and demonstration of vascular pathology," *Circulation* **93**(6), 1206–1213 (1996).
4. H. Yabushita, B. E. Bouma, S. L. Houser, H. T. Aretz, I. K. Jang, K. H. Schlendorf, C. R. Kauffman, M. Shishkov, D. H. Kang, E. F. Halpern, and G. J. Tearney, "Characterization of human atherosclerosis by optical coherence tomography," *Circulation* **106**(13), 1640–1645 (2002).
5. I. K. Jang, G. J. Tearney, B. MacNeill, M. Takano, F. Moselewski, N. Iftima, M. Shishkov, S. Houser, H. T. Aretz, E. F. Halpern, and B. E. Bouma, "In vivo characterization of coronary atherosclerotic plaque by use of optical coherence tomography," *Circulation* **111**(12), 1551–1555 (2005).
6. E. Grube, U. Gerckens, L. Buellesfeld, and P. J. Fitzgerald, "Images in cardiovascular medicine. Intracoronary imaging with optical coherence tomography: a new high-resolution technology providing striking visualization in the coronary artery," *Circulation* **106**(18), 2409–2410 (2002).
7. R. Huber, D. C. Adler, and J. G. Fujimoto, "Buffered Fourier domain mode locking: unidirectional swept laser sources for optical coherence tomography imaging at 370,000 lines/s," *Opt. Lett.* **31**(20), 2975–2977 (2006).
8. S. H. Yun, G. J. Tearney, B. J. Vakoc, M. Shishkov, W. Y. Oh, A. E. Desjardins, M. J. Suter, R. C. Chan, J. A. Evans, I. K. Jang, N. S. Nishioka, J. F. de Boer, and B. E. Bouma, "Comprehensive volumetric optical microscopy in vivo," *Nat. Med. (N.Y.)* **12**(12), 1429–1433 (2006).
9. J. Narula and J. T. Willerson, "Prologue: detection of vulnerable plaque," *J. Am. Coll. Cardiol.* **47**(8, Suppl), C1 (2006).
10. T. Kubo, T. Imanishi, S. Takarada, A. Kuroi, S. Ueno, T. Yamano, T. Tanimoto, Y. Matsuo, T. Masho, H. Kitabata, K. Tsuda, Y. Tomobuchi, and T. Akasaka, "Assessment of culprit lesion morphology in acute myocardial infarction: ability of optical coherence tomography compared with intravascular ultrasound and coronary angioscopy," *J. Am. Coll. Cardiol.* **50**(10), 933–939 (2007).
11. G. J. Tearney, I. K. Jang, and B. E. Bouma, "Optical coherence tomography for imaging the vulnerable plaque," *J. Biomed. Opt.* **11**(2), 021002 (2006).
12. I. K. Jang, B. E. Bouma, D. H. Kang, S. J. Park, S. W. Park, K. B. Seung, K. B. Choi, M. Shishkov, K. Schlendorf, E. Pomerantsev, S. L. Houser, H. T. Aretz, and G. J. Tearney, "Visualization of coronary atherosclerotic plaques in patients using optical coherence tomography: comparison with intravascular ultrasound," *J. Am. Coll. Cardiol.* **39**(4), 604–609 (2002).
13. D. Levitz, L. Thrane, M. Frosz, P. Andersen, C. Andersen, S. Andersson-Engels, J. Valanciunaite, J. Swartling, and P. Hansen, "Determination of optical scattering properties of highly-scattering media in optical coherence tomography images," *Opt. Express* **12**(2), 249–259 (2004).
14. M. J. Davies, "Stability and instability: two faces of coronary atherosclerosis. The Paul Dudley White Lecture 1995," *Circulation* **94**(8), 2013–2020 (1996).

15. A. I. Kholodnykh, I. Y. Petrova, K. V. Larin, M. Motamedi, and R. O. Esenaliev, "Precision of measurement of tissue optical properties with optical coherence tomography," *Appl. Opt.* **42**(16), 3027–3037 (2003).
16. F. J. van der Meer, D. J. Faber, D. M. Baraznji Sassoon, M. C. Aalders, G. Pasterkamp, and T. G. van Leeuwen, "Localized measurement of optical attenuation coefficients of atherosclerotic plaque constituents by quantitative optical coherence tomography," *IEEE Trans. Med. Imaging* **24**(10), 1369–1376 (2005).
17. F. J. van der Meer, D. J. Faber, J. Perree, G. Pasterkamp, D. Baraznji Sassoon, and T. G. van Leeuwen, "Quantitative optical coherence tomography of arterial wall components," *Lasers Med. Sci.* **20**(1), 45–51 (2005).
18. J. M. Schmitt, A. Knuttel, and R. F. Bonner, "Measurement of optical properties of biological tissues by low-coherence reflectometry," *Appl. Opt.* **32**(30), 6032–6042 (1993).
19. F. J. van der Meer, D. J. Faber, I. Cilesiz, M. J. van Gemert, and T. G. van Leeuwen, "Temperature-dependent optical properties of individual vascular wall components measured by optical coherence tomography," *J. Biomed. Opt.* **11**(4), 041120 (2006).
20. G. Marquez, L. V. Wang, S. Lin, J. A. Schwartz, and S. L. Thomsen, "Anisotropy in the absorption and scattering spectra of chicken breast tissue," *Appl. Opt.* **37**(4), 798–804 (1998).
21. T. Kume, T. Akasaka, T. Kawamoto, H. Okura, N. Watanabe, E. Toyota, Y. Neishi, R. Sukmawan, Y. Sadahira, and K. Yoshida, "Measurement of the thickness of the fibrous cap by optical coherence tomography," *Am. Heart J.* **152**(4), 755, e751–754 (2006).
22. S. D. Giattina, B. K. Courtney, P. R. Herz, M. Harman, S. Shortkroff, D. L. Stamper, B. Liu, J. G. Fujimoto, and M. E. Brezinski, "Assessment of coronary plaque collagen with polarization sensitive optical coherence tomography (PS-OCT)," *Int. J. Cardiol.* **107**(3), 400–409 (2006).
23. S. K. Nadkarni, M. C. Pierce, B. H. Park, J. F. de Boer, P. Whittaker, B. E. Bouma, J. E. Bressner, E. Halpern, S. L. Houser, and G. J. Tearney, "Measurement of collagen and smooth muscle cell content in atherosclerotic plaques using polarization-sensitive optical coherence tomography," *J. Am. Coll. Cardiol.* **49**(13), 1474–1481 (2007).
24. B. Liu and M. E. Brezinski, "Theoretical and practical considerations on detection performance of time domain, Fourier domain, and swept source optical coherence tomography," *J. Biomed. Opt.* **12**(4), 044007 (2007).